A new automatic approach for extracting glacier centerlines based on Euclidean allocation

Dahong Zhang[1,2], Xiaojun Yao[1,3], Hongyu Duan[1], Shiyin Liu[4], Wanqin Guo[5], Meiping Sun[1], Dazhi Li[1]

[1]College of Geography and Environment Sciences, Northwest Normal University, Lanzhou, China

5   [2]College of Urban and Environmental Sciences, Northwest University, Xi'an, China

[3]National Cryosphere Desert Data Center, Lanzhou, China

[4]Institute of International Rivers and Eco-security, Yunnan University, Kunming, China

[5]State Key Laboratory of Cryospheric Science, Northwest Institute of Eco-Environment and Resources, Chinese Academy of Sciences, Lanzhou, China

10   *Correspondence to*: Xiaojun Yao (yaoxj_nwnu@163.com)

Abstract. Glacier centerlines are crucial input for many glaciological applications. From the morphological perspective, we proposed a new automatic method to derive glacier centerlines, which is based on the Euclidean allocation and the terrain characteristics of glacier surface. In the algorithm, all glaciers are logically classified as three types including simple glacier, simple compound glacier and complex glacier, with corresponding process ranges from simple to complex. The process for

15   extracting centerlines of glaciers introduces auxiliary reference lines, and follows the setting of not passing through bare rock. The program of automatic extraction of glacier centerlines was implemented in Python and only required glacier boundary and digital elevation model (DEM) as input. Application of this method to 48571 glaciers in the second Chinese glacier inventory automatically yielded the corresponding glacier centerlines with an average computing time of 20.96 s, a success rate of 100% and a comprehensive accuracy of 94.34%. A comparison of the longest length of glaciers to the corresponding glaciers in the

20   Randolph Glacier Inventory v6.0 revealed that our results were superior. Meanwhile, our final product provides more information about glacier length, such as the average length, the longest length, the lengths in the accumulation and ablation regions of each glacier.

1 Introduction

Glaciers are an important freshwater resource on earth and a vital part of the cryosphere (Muhuri et al., 2015). According to the Fifth Assessment Report (AR5, https://www.ipcc.ch/) published by the Intergovernmental Panel on Climate Change (IPCC), there are 168331 glaciers (including ice caps) in the world, with a total area of 726258 km^2 apart from ice sheets. Glaciers move towards lower altitude by gravity, which is the most obvious distinction between glacier and other natural ice bodies. The glacier flowlines are the motion trajectories of a glacier, and the main flowline is the longest flow trajectory of glacier ice. Due to the differences in the speed and moving direction of any point at the surface or inside the glacier, the calculation of the main flowline of glaciers requires a coherent velocity field data, which is difficult to obtain on the global or regional scale (McNabb et al., 2017). Therefore, some concepts such as the glacier axis and the glacier centerlines were proposed (Le Bris and Paul, 2013; Kienholz et al., 2014; Machguth and Huss, 2014). Glacier centerlines are the central lines close to main flowlines of glaciers, which can be acquired based on glacier axis and be used to simulate glacier flowline.

As an important model parameter, the glacier centerline can be used to determine the change of glacier length (Leclercq et al., 2012a; Nuth et al., 2013), analyze the velocity field (Heid and Kääb, 2012; Melkonian et al., 2017), estimate the glacier ice volume (Li et al., 2012; Linsbauer et al., 2012), and develop one-dimensional glacier models (Oerlemans, 1997; Sugiyama et al., 2007). Meanwhile, the length of the longest glacier centerline is one of the key determinants of glacier geometry and an important parameter of glacier inventory (Paul et al., 2009; Leclercq et al., 2012b). The length and area of glacier can be also used to estimate the large-scale glacier ice volume (Zhang and Han, 2016; Gao et al., 2018). The length change at the terminus of a glacier can directly reflect the state of motion, e.g., glacier recession, glacier advance or surging (Gao et al., 2019). Winsvold et al. (2014) analyzed the changes of glacier area and length in Norway, using glacier inventories derived from Landsat TM/ETM+ images and digital topographic maps. Herla et al. (2017) explored the relationship between the geometry and length of glaciers in the Austrian Alps based on a third-order linear glacier length model. Leclercq et al. (2012, 2014) reconstructed annual averaged surface temperatures in the past 400 years on hemispherical and global scale from glacier length fluctuations. These studies indicated that both the extraction of contemporary glacier length and the reconstruction of historical glacier length require more accurate extraction methods of glacier flowlines.

In order to obtain the length of glaciers, some automatic or semi-automatic methods were proposed in recent years. Schiefer et al. (2008) extracted the longest flow path on the ice surface based on a hydrological model, which was generally 10% to 15% larger than the glacier length. Le Bris et al. (2013) accomplished the automatic extraction of flow lines from the highest point to the terminus of a glacier based on the concept of glacier axis, with a verification accuracy of 85%. Unfortunately, the branches of glacier centerlines have not been extracted and the length is not necessarily the maximum for huge or complex glaciers (Paul et al., 2009). Machguth et al. (2014) proposed an extraction method of glacier length based on the slope and width of glacier with a success rate of 95-98%, however the branches of glacier centerlines could not be extracted either. Kienholzs et al. (2014) applied the grid–least-cost route approach to the automatic extraction of glacier flow lines, having an automation degree of 87.8% with additional manual intervention. Yao et al. (2015) proposed the semi-automatic method of extraction glacier centerlines based on Euclidean allocation theory, which required the expertise and experiences for composite valley glaciers and ice caps. So, the current biggest challenge is still the implementation of automation extraction of glacier centerline and the acquirement of more information about glacier length. The aims of this study are to design an algorithm to: (i) automatically generate centerlines for the main body of each glacier and its branches; (ii) automatically calculate the longest length, average length, the length of accumulation region, and the length of ablation region of each glacier, along with corresponding polylines; and (iii) improve the degree of automation as much as possible on the premise of ensuring the accuracy of glacier centerlines.

2 Input data and test region

The glacier dataset used in this study is the Second Chinese Glacier Inventory (SCGI) released by National Tibetan Plateau Data Center (http://westdc.westgis.ac.cn/data), which has been approved by some organizations (e.g., WGMS, GLIMS, NSIDC, etc.) and adopted in the Randolph Glacier Inventory (RGI) v6.0 (Guo et al., 2017). According to the SCGI (Fig.1), there were 48571 glaciers in China, with a total area of 51766.08 km^2, accounting for 7.1% of the glacier area in the world except for the Antarctic and Greenland ice sheets (Liu et al., 2015). Due to the lack of automatic method to calculate glacier's length, there was no length property in the SCGI, and some subsequent studies haven't made great breakthroughs (Yang et al., 2016; Ji et al., 2017).

The SCGI was produced based on Landsat TM/ETM+ images and ASTER images in the period of 2004-2011 and SRTM v4.1 with a spatial resolution of 90 m (Liu et al., 2015). In this study, we selected SRTM1 DEM v3.0 (http://www2.jpl.nasa.gov/srtm, last accessed on March 2, 2013, with a spatial resolution of 30 m) (Farr et al., 2007) in consideration of its free access and higher data quality, which was used to identify division points on the glacier outlines, extract ridge lines in the coverage region of glaciers, and generate the glacier centerlines. Additionally, we extracted glaciers in China from the RGI v6.0 provided by GLIMS (http://www.glims.org/RGI/). There are 38053 glaciers matching the graphic position of the SCGI. The field of L_{max} of RGI v6.0 provides the length of the longest flowlines on the glacier surface, which was calculated with the algorithm proposed by Machguth et al. (2014). For verifying the validity and accuracy of glacier centerlines, we compared the extracted longest length of glaciers with the value of L_{max} in the RGI v6.0.
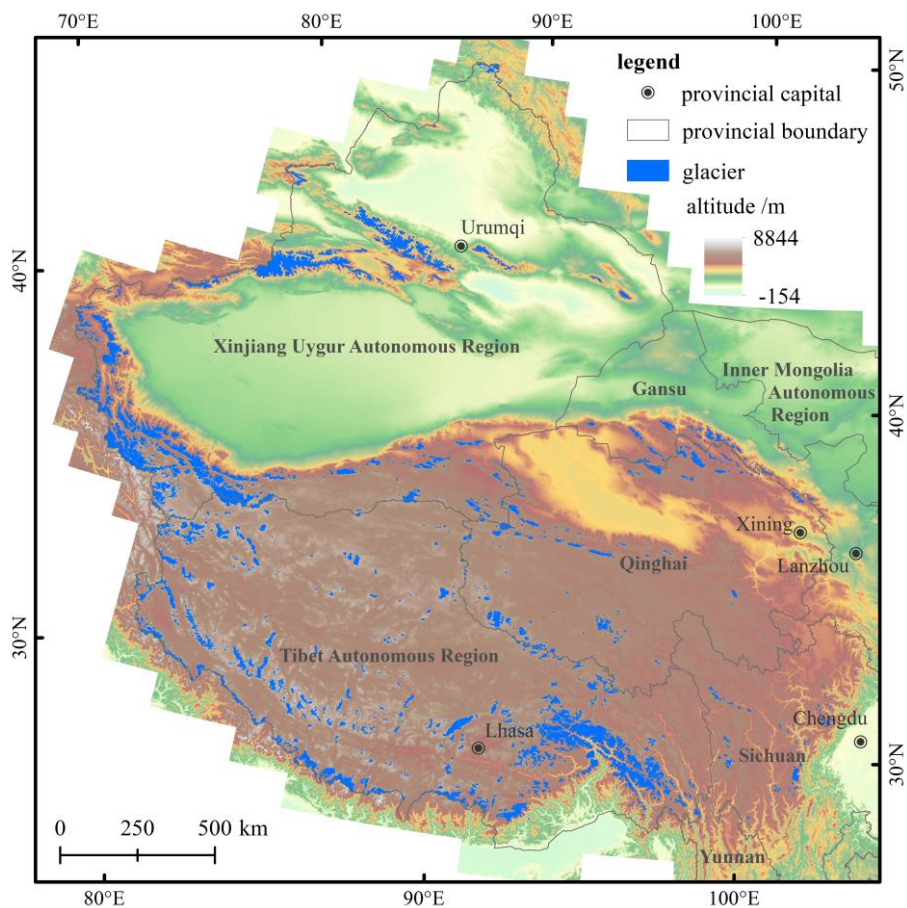
Figure 1: The distribution of glaciers in China.

3 Principles and algorithm of glacier centerline extraction

In order to implement the automatic extraction of glacier centerlines, we have designed a new set of algorithms. Relevant parameters and processing procedures are introduced as follows.

3.1 Model parameters

The code was written in Python and partially invoked the site package of ArcPy. The calculation of the glacier centerlines relies on two basic inputs: (i) glacier in the form of polygon with a unique value field and a projection coordinate system (unit: m), (ii) DEM data having the spatial resolution and acquisition time close to the images used for glacier inventory. We defined 11 adjustable parameters named P_i (i=1,…,11) (see Table 1), which were achieved by classifying glacier polygon through a set of reasonable rules. The purpose is to improve the degree of automation and the accuracy. Three key parameters are described as:

—P_3: the threshold of flow accumulation, to control the generation of auxiliary lines.

—P_6: the step size of searching the local highest points, to control the extraction of extremely high points.

—P_8: The grid cell size of Euclidean allocation, to improve the algorithm efficiency.

In the algorithm, the number of the local highest points is affected by the perimeter of the glacier (P_g). We took the given area (A_t) and the perimeter (P_t, Eq.1) of the equilateral triangle corresponding to A_t as the grading threshold. According to the area (A_g) and the perimeter (P_g) of each glacier's outer boundary, all glaciers were divided into five levels (Eq.2), which represented the five levels of glacier polygon with difference in P_g. The built-in parameters were set according to the different levels (Table 1). P_4, P_5 and P_9 were controlled in proportion to the side length of the equilateral triangle corresponding to P_t. The proportional coefficient was T (Eq.3). According to the actual situation of the repeated programing test, the empirical value of each parameter is given in Table 1.

$$P(A_t) = 2 \times 3^{0.75} \times A_t^{0.5} \tag{1}$$

$$L(A_g, i) = \begin{cases} i: A_g \in [A_{i-1}, A_i) \text{ and } P_g \in [P(A_i), +\infty) \text{ and } i \in (1,5] \\ i: A_g \in [A_i, A_{i+1}) \text{ and } P_g \in [P(A_i), P(A_{i+1})) \text{ and } i \in [1,5] \\ i: A_g \in [A_{i+1}, A_{i+2}) \text{ and } P_g \in (0, P(A_{i+1})) \text{ and } i \in [1,5) \\ 0: \text{ the above conditions aren't met} \end{cases} : \begin{matrix} A = \{0,1,5,20,50, +\infty\} \\ i = \{1,2,3,4,5\} \end{matrix} \tag{2}$$

$$f(T) = \frac{P_g}{3 \times 2 \times T} \qquad (3)$$

Table 1 The description of adjustable parameters.

Levels	1	2	3	4	5	Parameter elucidation
Par.	L(A_g,1)	L(A_g,2)	L(A_g,3)	L(A_g,4)	L(A_g,5)	
*P_1			"10 meters"			Maximum distance between adjacent vertexes of polyline
*P_2			"30 meters"			Buffer distance outside the glacier outline
P_3	500	600	700	800	800	The threshold of accumulative flow
P_4	$f(10)$	$f(11)$	$f(12)$	$f(13)$	$f(15)$	The length of the shortest auxiliary line
P_5	$f(2)$	$f(3)$	$f(4)$	$f(5)$	$f(6)$	The length of the longest auxiliary line
P_6	50	60	70	80	80	The interval for searching the local highest points
P_7	0.2	0.2	0.5	0.5	1	The matching tolerance of the vertexes of polyline
P_8	1	5	15	15	30	The size of grid cell in Euclidean allocation
P_9	$f(10)$	$f(15)$	$f(30)$	$f(60)$	$f(120)$	Minimum distance between the adjacent local highest points
P_{10}	5	10	15	20	30	The smoothing tolerance of polylines
*P_{11}			P(A_t=5)			Threshold to control the length of the longest auxiliary line

Note: the parameters with "*" are constant.

3.2 Computation flow

In this paper, glaciers were divided into three categories: simple glacier (extremely high point: single, auxiliary line: no, the area of bare rock: no), simple compound glacier (extremely high point: several, auxiliary line: no, the area of bare rock: no), and complex glacier (extremely high point: several, auxiliary line: yes, the area of bare rock: yes). Following the principle from simple to complex, the algorithm was composed of six main steps: data preprocessing, extraction of auxiliary lines, identification of division points, reconstruction of feature lines, extraction of centerlines and the calculation of glacier length. The flow chart of the algorithm is illustrated in Fig.2.

The automatic extraction of glacier centerlines in this study obeys the following rules: (i) the elevation of the local highest points must be higher than the equilibrium line altitude (ELA), (ii) a glacier has only one exit, which is the lowest point of the polyline of the glacier's outer boundary (G_{pl}); (iii) the auxiliary line only acts on the accumulation region of glacier; (iv) the G_{pl}, auxiliary lines, and bare rock region simultaneously serve as barrier lines to restrict the flow direction of the glacier centerlines.
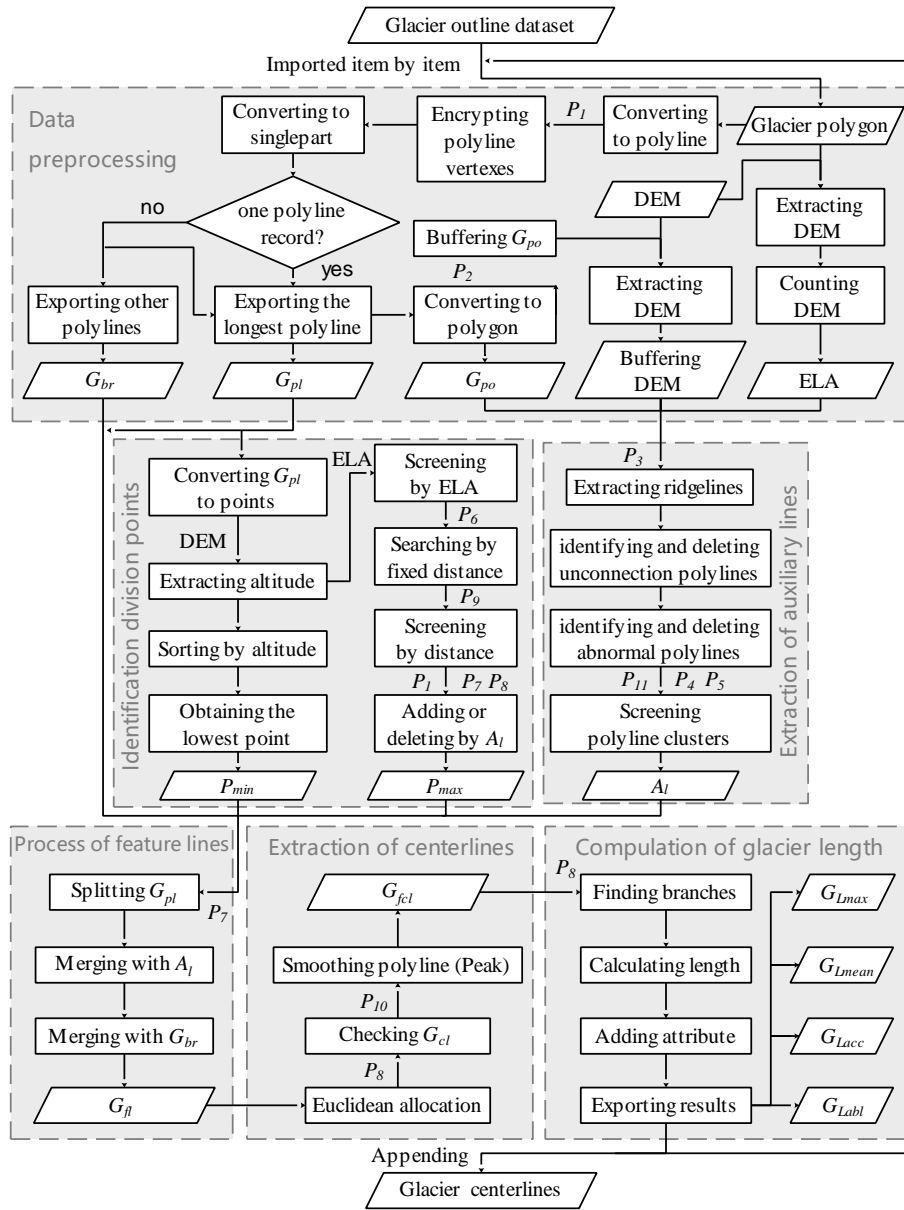
Figure 2: The flow chart of algorithm.

3.3 Critical processes

3.3.1 Data preprocessing

125   The data preprocessing includes four parts: (i) checking the input data, (ii) pre-processing the glacier outlines, (iii) fine-tuning

the built-in parameters, and (iv) calculating the ELA of glaciers. First, the polygon of the glacier's outer boundary (G_{po}), the polyline of glacier's outer boundary (G_{pl}) and the boundary of the bare rock in glacier (G_{br}) were obtained by splitting the glacier outlines in the importing module. These temporary data would be used as the input parameters of other modules in subsequent process. Secondly, the module exported the number of closed lines in glacier outlines, A_g and P_g, which were used to determine the number of bare rocks on the glacier surface, the type and level of glaciers. Thirdly, according to the parameter adjusting rules at the level of glaciers, 11 built-in parameters (see Table 1) were fine-tuned. Finally, the median elevation (Z_{med}) of each glacier aided by its DEM was computed, which was then used to estimate the ELA of each glacier. The schematic diagram of processing glacier outlines is shown in Fig.3.
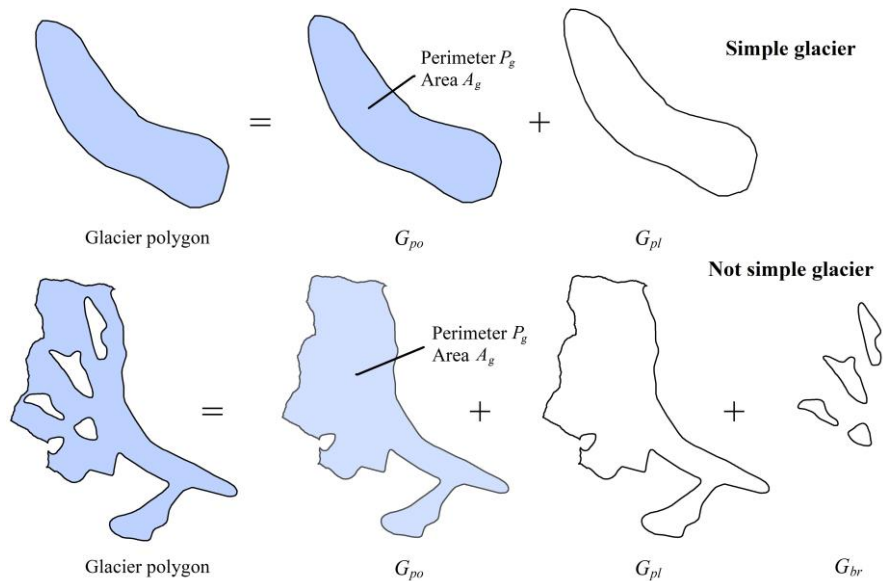
Figure 3: The schematic of processing raw data (G_{po} denotes the polygon of the glacier; G_{pl} denotes the polyline of glacier's outer boundary; and G_{br} denotes the boundary of the bare rock in glacier).

3.3.2 Extraction of auxiliary lines

For making glacier centerlines more reasonable, we introduced the auxiliary lines that represent the internal ridgelines of glaciers to intervene in the generation of centerline for the upper part of a glacier. The extraction of auxiliary lines included the extraction of ridgelines and post-processing. Based on the inverse terrain method, the extraction of ridgelines was easily

accomplished by the workflow of hydrologic analysis. The post-processing was relatively complicated. The main reason was that the auxiliary lines were tree-like polylines starting from the upper boundary of the glacier. In principle, the mass flow in the location of the auxiliary lines on the glacier surface could be obviously blocking-up, which was equivalent to the ice divide. The preliminary ridgelines needed to be screened once more combining with DEM by traversal method. Determining the cluster of auxiliary lines was the main problem to be solved by the algorithm of this part. According to the designed algorithm, it could be divided into five parts in post-processing: (i) identifying and deleting the disconnected lines, (ii) identifying and deleting the abnormal lines, (iii) determining the members of line cluster, (iv) determining the longest length of line cluster, and (v) screening the line clusters. The schematic diagram of extracting the auxiliary lines is shown in Fig.4.
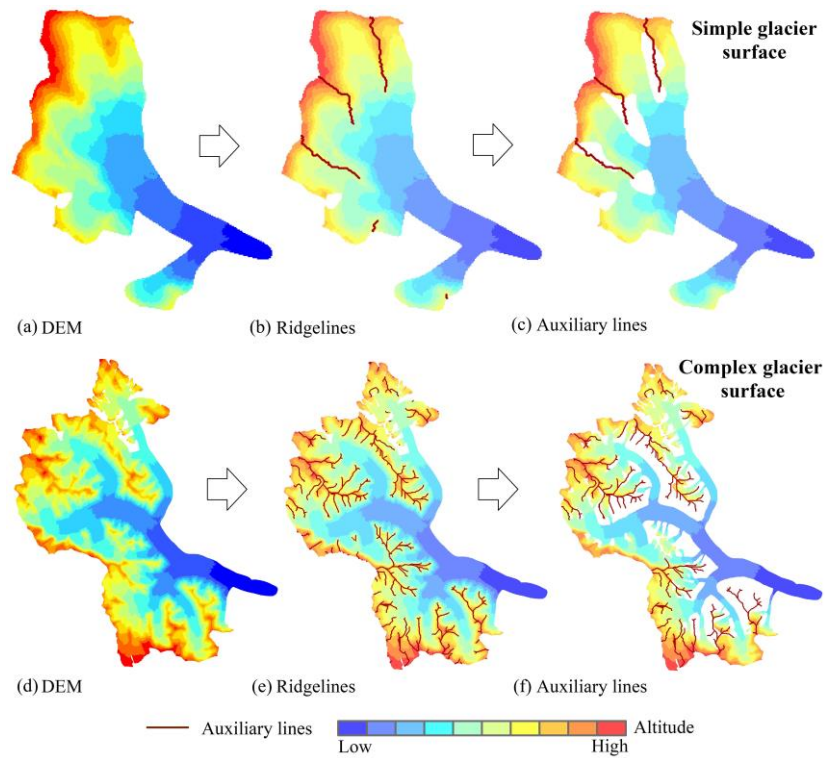
Figure 4: The schematic of extracting auxiliary lines. (a) and (d) demonstrate the digital elevation model (DEM) around the glacier; (b) and (e) show the ridgelines in region covered by DEM; (c) and (f) show the auxiliary lines in glacier.

The automatically extracted ridgelines were often disconnected, so it was necessary to remove independent existence or unreasonable ridgelines using the auxiliary data such as DEM, ELA and G_{po} by ergodic algorithms. Firstly, the ridgelines of

the glacier surface (A_r) were obtained by clipping the ridge lines using G_{po}. The set of all possible starting points of auxiliary lines was gained by intersecting A_r with G_{pl}. Then, the ridgeline clusters connected to each starting point were achieved and marked by traversing the point set. The number of auxiliary lines was initially determined. Lastly, the longest length of each auxiliary line was calculated by adopting the critical path algorithm. The final auxiliary lines (A_l) were obtained by screening all auxiliary lines using the three parameters of P_4, P_5 and P_{11}.

3.3.3 Identification of division points

The division points include the lowest point (P_{min}) and the local highest point (P_{max}). The ordered point set (h) was obtained after converting G_{pl} from a polyline to a point set and extracting the elevation for the point set. The method for obtaining P_{min} was relatively simple, as showed in Eq. (4).

$$P_{min} = Min(h_1, h_2, \cdots, h_n) \tag{4}$$

In comparison, the extraction of P_{max} was more complicated. It was necessary to ensure the extraction of all possible branches of the centerlines and avoid the redundancy of branches. The algorithm could be divided into four steps: (i) obtaining the local highest point set (M″) by filtering h (Eq.5, Eq.6) according to P_6, (ii) removing the elements (Eq.7) at an altitude lower than ELA from M″, (iii) removing the elements (Eq.8) of adjacent distance less than P_9 from M′, and (vi) checking, deleting or adding some local highest points (Eq.9) using the auxiliary lines to ensure that there was at least one local highest point among adjacent auxiliary lines.

$$H_i = \left\{ h_{i-\frac{P_6}{2}}, \cdots, h_{i-1}, h_i, h_{i+1}, \cdots, h_{i+\frac{P_6}{2}} \right\}, i \in \left[\frac{P_6}{2}, n - \frac{P_6}{2} \right] \tag{5}$$

$$M'' = \{ h_i | h_i \geq Max(H_i) \} \tag{6}$$

$$M' = \left\{ M_j'' \middle| M_j'' \geq ELA \right\}, j \in [0, card(M'')) \tag{7}$$

$$M = \{ M_k' | d(M_{k-1}', M_k') \geq P_9, and\ d(M_k', M_{k+1}') \geq P_9 \}, k \in [0, card(M')) \tag{8}$$

$$P_{max} = M \cup \{ l_j | l_j \geq Max(L_i) \} \tag{9}$$

3.3.4 Reconstruction of feature lines

Feature lines of glacier surface were used to express G_{pl}, G_{br}, A_l, P_{max}, P_{min}, and the intersection of A_l and G_{pl}. The schematic

diagram of merging the glacier surface features is illustrated in Fig.5.
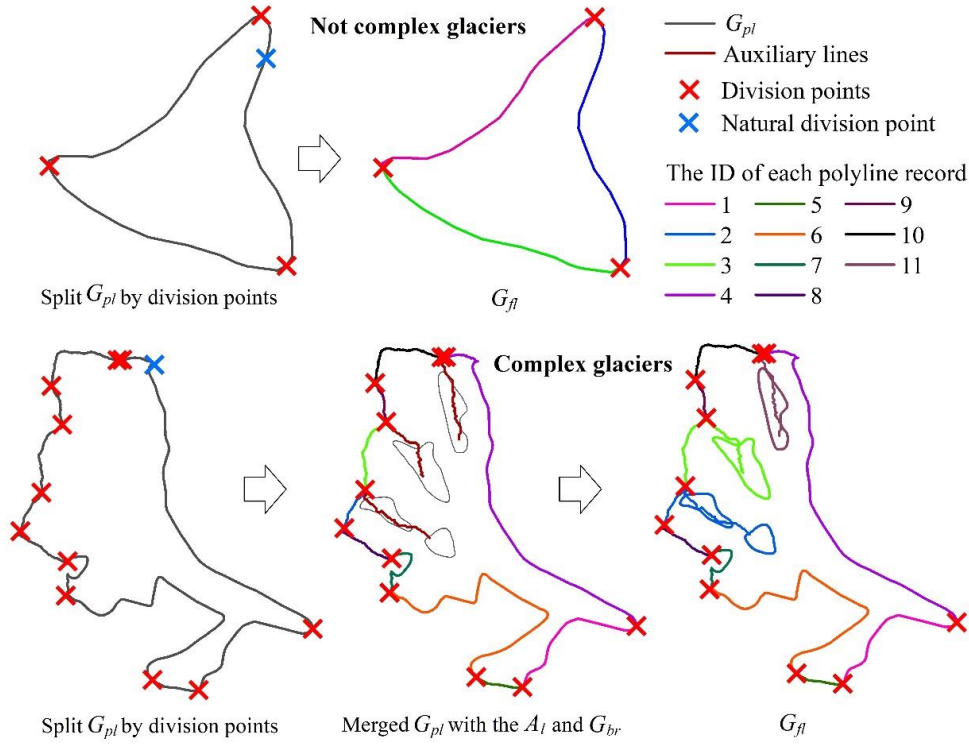
Figure 5: The schematic of extracting the polyline features of glacier surface.

For simple glaciers and simple compound glaciers, it was only necessary to merge P_{max} and P_{min} into a vector file, then split G_{pl}, and allocate one unique code for each polyline after converting it from multipart to singlepart. For complex glacier, the processing method was composed of several steps. First of all, the G_{pl} split by division points needed to be combined with G_{br} (if any) and A_l (if any) into a vector file. After converting it from multipart to singlepart, program would allocate again code for each polyline and remark it as G_{sp1}. Secondly, polyline records in G_{sp1} were selected one by one with A_l, and then the polyline records belonging to the same part in G_{sp1} were merged, which was recorded as G_{sp2}. Thirdly, G_{edge} was exported by selecting G_{sp2} using G_{pl}, and G_{alone} was exported after switching selection, which represented the bare rock region that still existed independently after merging the glacier outlines with the auxiliary lines. Finally, adopting the proximity algorithm, each element (if any) in G_{alone} was processed in turn with G_{edge}. Specifically, it needed three steps: (i) The vertex set E (Eq.10) of G_{edge} and the vertex set U (Eq.11) of G_{alone} were obtained. (ii) The pairs of polylines (Eq.12) matched by serial number were

calculated and made the corresponding marks in G_{sp2}; (iii) The feature lines (G_{fl}) of glacier surface were reconstructed by merging the same marks in G_{sp2}.

$$E_i = \{E_{ij} | j \in [0, card(E)\}$$ (10)

$$U_p = \{U_{pq} | q \in [0, card(U)\}$$ (11)

195 $$D = \{(p, i) | Min\left(d(U_p, E_i)\right)\}$$ (12)
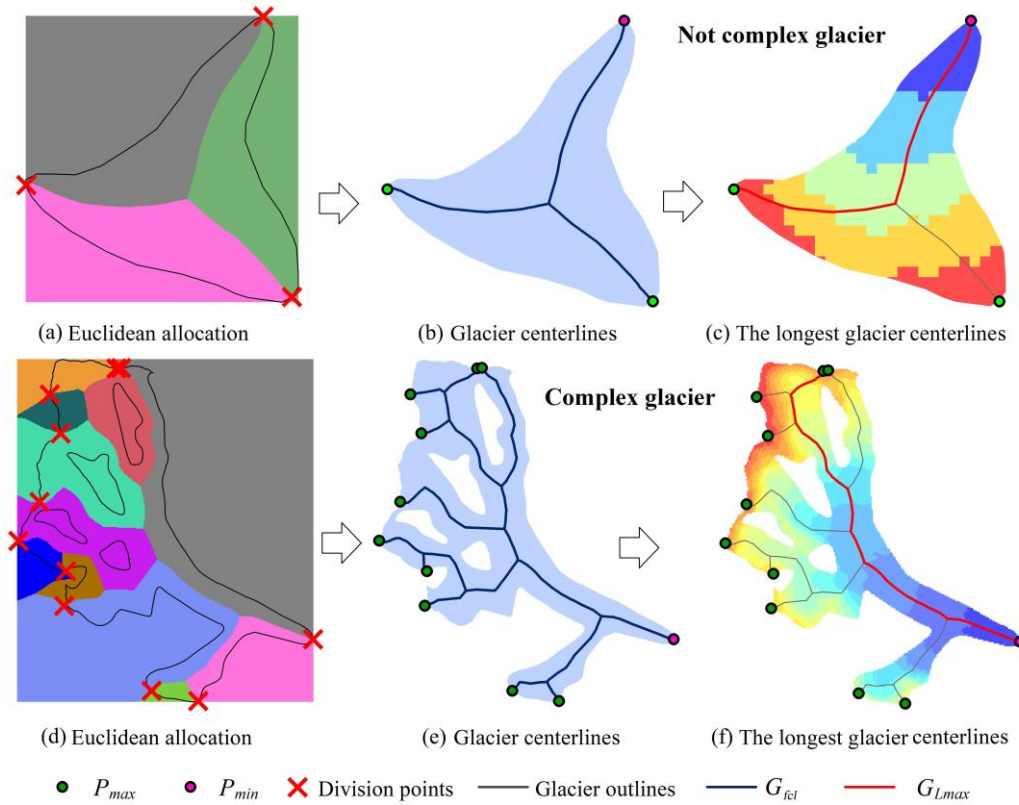
Figure 6: The schematic of extracting centerlines and the longest centerline of the glacier. (a) and (d) show the results after executing the European allocation, and the different colors represent the regions which have the shortest distance to the corresponding edges of the glacier; (b) and (e) represent the centerlines(G_{fcl}), the local highest point (P_{max}) and lowest point (P_{min}) of the glacier; (c) and (f) demonstrate the longest centerline (G_{Lmax}) of the glacier and the background is the digital elevation model with the graduated red (high)– blue (low) color.

3.3.5 Extraction of glacier centerlines

Original glacier centerlines (G_{cl}) were achieved with the function of Euclidean allocation in ArcPy, which needed the input of G_{fl} and set the value of P_8. Firstly, the feature lines (G_{fl}) after automatically deriving by the program are input, and the function of Euclidean allocation in ArcPy is called to generate the division glacier surface. Then the common edges between regions on the dividing glacier surface are identified. Finally, the common edges are automatically checked and processed to obtain G_{cl}. The final glacier centerlines (G_{fcl}) were obtained by processing G_{cl} with Peak algorithm, after setting the tolerance for smoothing polylines (P_{10}). The schematic diagram of extracting G_{fcl} and the longest length of glaciers (G_{Lmax}) is shown in Fig.6.

3.3.6 Calculation of glacier length

The final code of the G_{fcl} was determined by P_{min} after G_{fcl} being converted from multipart to singlepart and was given in a unified format. Then all branches of glacier centerlines and glacier length were achieved using algorithm (Fig.7) similar to the critical path. This work consisted of four steps: (i) the polyline set of G_{fcl} was recorded as C (Eq.13), then the sets of polyline length (L) and polyline endpoint (S) (Eq.13) were obtained; (ii) the initial search point (B) (Eq.14), the end of glacier centerline, was determined by the coordinates of P_{min} based on the above steps. The common endpoint set (N) (Eq.14) with the next parts of glacier centerlines was obtained, and then the polyline code corresponding to B was recorded; (iii) each element in N was used as a new starting point for search respectively (B') (Eq.15), which was used to get the common endpoint set (N') (Eq.15) with the next parts of glacier centerlines. The coding of the corresponding polyline set of each glacier branch was recorded separately and (vi) the above process continued until all branches of glacier centerline trace back to its corresponding P_{max} (Eq.16).

$$C_i = \{C_{ij} | j \in [0, card(C)\}$$
$$S = \{(s_i, e_i) | s_i = C_{[i][0]}, and\ e_i = C_{[i][card(C_i)-1]}\} \tag{13}$$

$$B = \{k | P_{min} \in S_k\}, k \in [0, card(S))$$
$$N = \{P | P \neq P_{min}, and\ P \in S_B\} \tag{14}$$

$$B' = \{k | N \in S_k, and\ k \neq B\}, k \in [0, card(S))$$
$$N' = \left\{P \middle| P \neq N, and\ P \in S_{B'_m}\right\}, m \in [0, card(B')) \tag{15}$$

$$res = \{\{a, b, d\}, \{a, b, e\}, \{a, c, f, h\}, \{a, c, g\}, \{a, c, f, t\}\} \tag{16}$$
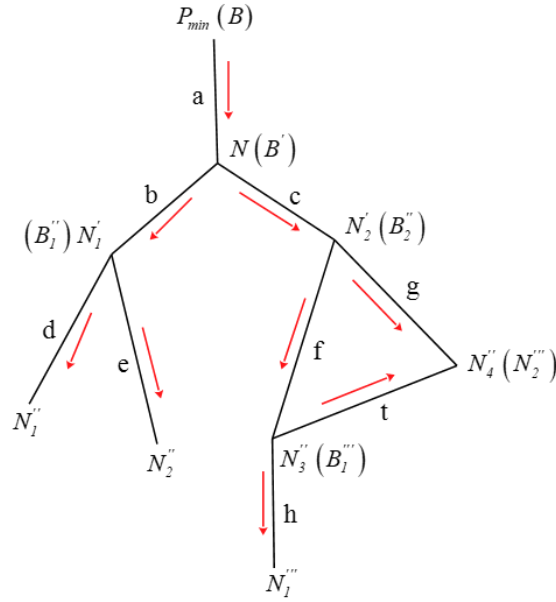
Figure 7: The schematic of calculating glacier length (The red arrow represents the search direction of the branches of glacier centerline).

The length of each branch of glacier centerlines was counted. The average length (Eq.17) of all branches was named as the average length of a glacier (G_{Lmean}). The longest length (Eq.18) of all branches was named as the longest length of a glacier (G_{Lmax}). In addition, the part above ELA in G_{Lmax} was regarded as the accumulation region length (G_{Lacc}) of a glacier, and the part of G_{Lmax} with altitude lower than ELA was regarded as the ablation region length (G_{Labl}) of a glacier. Finally, the corresponding vector data were generated and some attributes including the corresponding polyline code, glacier code, the value of glacier length were added.

$$L_{mean} = \frac{SUM(Lres_i)}{card(res)} \tag{17}$$

$$L_{max} = Max(Lres_i) \tag{18}$$

4 Accuracy evaluation and the results

4.1 Methods of quality analysis

Here, we used the SCGI as the test data to run the designed program, including 48571 glaciers. The extraction results of some

typical examples of glaciers (from simple to complex) are presented in Fig.8. The accuracy of glacier centerlines was evaluated based on a random verification method in this study. All glaciers (total quantity: N_G) corresponding to the samples were obtained and arranged in ascending order of the area. Specifically, 100 random integers were generated in the set of [0, N_G). Glaciers with corresponding serial number were exported as samples. After the visual inspection, the accuracy evaluation was conducted based on the following statistical analysis.
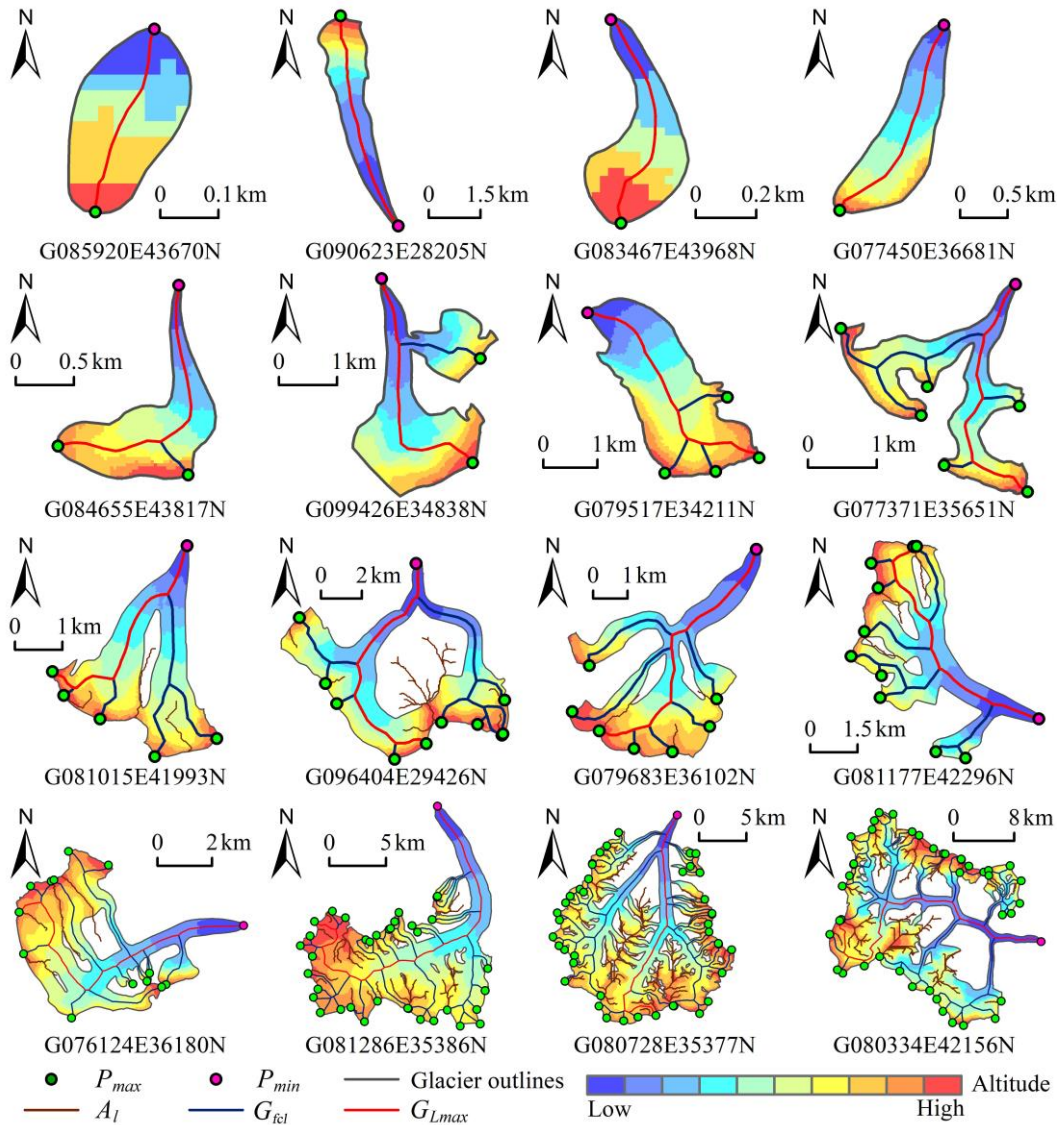
Figure 8: The centerlines for some typical glaciers (P_{max} and P_{min} denote the local highest point and lowest point in the boundary of the glacier, respectively; A_l denotes the auxiliary lines; G_{fcl} and G_{Lmax} denote the centerlines and the longest centerline of the glacier).

Firstly, 100 glaciers were randomly selected from the glacier dataset as samples to obtain a verification accuracy (R_1) (Eq.19).

Secondly, each level of glaciers was separately taken as the total (N_T), and 100 glaciers were randomly selected. There were 5 samples for 5 levels, which were used to calculate a verification accuracy (R_2) (Eq.20) by taking the number proportion of each glacier level as the weight. Then, 100 glaciers with the largest, middle and smallest areas were selected separately as

samples. The verification accuracy (R_3) (Eq.21) was derived using 1:2:1 as the allocation proportion of weight. Finally, the average value of R_1, R_2 and R_3 was used as the comprehensive accuracy (R) (Eq.22). Among them, S_i represented the verification accuracy of the *ith* sample (i = {1,2,3,4,5,6,7,8,9}).

$$R_1 = S_1 \tag{19}$$

$$R_2 = \sum_{i=5}^{9} \frac{S_i \times N_{T_i}}{N_G} \tag{20}$$

$$R_3 = 0.25 \times S_2 + 0.5 \times S_3 + 0.25 \times S_4 \tag{21}$$

$$R = \frac{R_1 + R_2 + R_3}{3} \tag{22}$$

4.2 Sample selection and assessment criteria

Visual inspection in combination with satellite images and topographic maps is the most direct evaluation method for extraction results. Using 48571 glaciers in China as the test data, nine samples of 900 glaciers were selected for three verifications according to the evaluation method defined in section 4.1. The samples used for verification and relative information are given in Table 2.

Table 2 The information about validation samples.

Verification identifier	1-whole		2-area				3-levels		
Sample identifier	a	b	c	d	e	f	g	h	i
Selection conditions	Random	Max.	Central	Min.			Random		
Sample number	100	100	100	100	100	100	100	100	100
Total amount	48571		48571		38463	7341	2061	501	205
Proportion of sample (%)	0.21		0.62		0.26	1.36	4.85	19.96	48.78
Proportion of total (%)	100		100		79.19	15.11	4.24	1.03	0.42

Considering the possible defaults of the input data, we set some standards of accuracy evaluation (Table 3). The first level includes three categories: correct (I), inaccurate (II) and incorrect (III). The secondary categories were divided into 11 categories according to probable causes, among which the inaccurate causes and incorrect causes were subclassified as 6 types and 4 types, respectively. Type II involves mostly glaciers with accurate G_{Lmax} but missing, redundant or unreasonable branches of glacier centerlines. When calculating the comprehensive accuracy, category I and II were regarded as correct, and only III

was considered incorrect.

Table 3 The rules of accuracy assessment.

1st-level categories		2nd-level categories	
Code	Descriptions	Code	Descriptions
I	Correct	11	Correct
		21	Inaccurate glacier outlines
		22	Inaccurate identification of extreme points
		23	Inaccurate proximity algorithm for bare rock regions
II	Inaccurate	24	The influence of shunt or convergence in the glacier centerlines
		25	Inaccurate ridgelines
		26	Others (issues that are unknown by the algorithm itself, glaciers or DEM data)
		31	Undivided glaciers
		32	Ice caps
III	Incorrect	33	Slope glacier, i.e., glaciers with little change in slope
		34	Others (unknown issues by the algorithm itself, issues with glaciers and DEM data, indistinguishable glacier types, etc.)

4.3 Statistics of different samples

According to the standards in Table 3, the selected samples were conducted with visual investigation. The results of nine samples were displayed in Fig.9. The statistical results showed that the accuracy of verification-2 was the highest (95.25%), followed by the verification-3 (94.76%) and the verification-1 (93%). The comprehensive accuracy of glacier centerlines was 94.34%, of which category-I and category-II accounted for 86.06% and 8.28%, respectively. Meanwhile, we summarized the frequency of each type in each sample basing on 2nd-level categories. As seen in Fig.10, the problems of centerlines of small glaciers were mainly caused by the inaccurate selection of division points due to the insufficient accuracy of DEM (code: 22) and incorrect calculation results of some glaciers with little change in slope (code: 33). The problems of centerlines of large glaciers were mainly concentrated in some types coded in 31 and 32, which needed to be repartitioned and recalculated. In addition, a few problems were found in samples: the upper outlines of glacier were across the ridgeline; a small number of glaciers were not correctly segmented; the altitude in glaciers' DEM was abnormal. It implied that the reasonable glacier outlines and accurate DEM data were the prerequisite for extracting glacier centerlines and calculating glacier length.
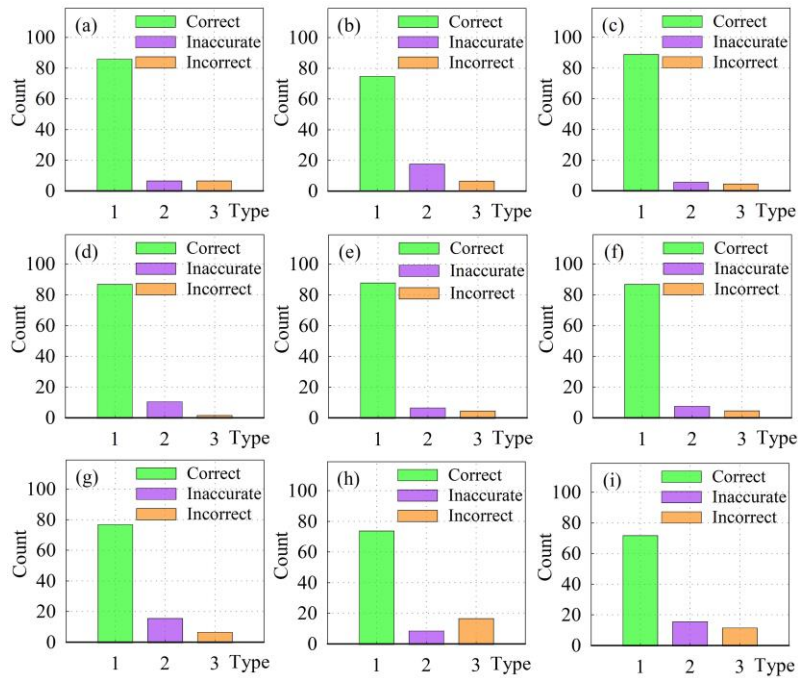
Figure 9: The statistical chart of evaluating results according to the 1st-level categories.

285
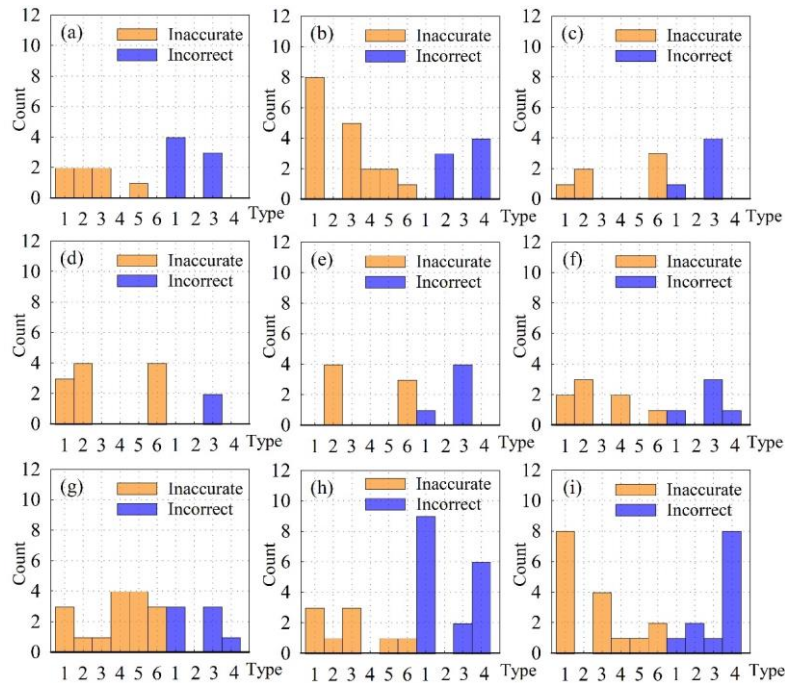
Figure 10: The statistical chart of evaluating results according to the 2nd-level categories.

4.4 Comparison to glaciers' maximum length from the RGI v6.0

4.4.1 The statistic of bit order and D_L

In the RGI v6.0, 38053 glaciers in the SCGI were adopted and accounted for 78.35% of the total glaciers in China, by checking the GLIMS_ID in both glacier datasets. As mentioned above, the field L_{max}, the longest glacier length, was contained in the RGI v6.0. In order to further verify the accuracy of glacier length calculated by this method, we calculated the difference (D_L) between G_{Lmax} and L_{max}, and then arranged them in ascending order to generate the distribution diagram of sequence-D_L (Fig.11). If D_L was negative, it meant that the G_{Lmax} of glaciers with the corresponding serial number was smaller than L_{max} and vice versa. Overall, there were only a small part of glaciers with extremely large $|D_L|$ at both ends (Fig.11). After visual inspection, G_{Lmax} was more consistent with the actual status of glaciers.
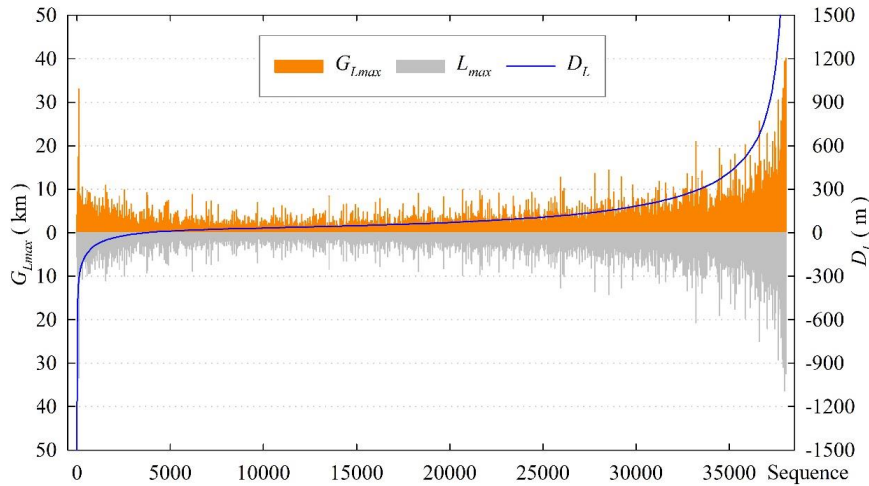
Figure 11: The statistical chart of the difference (D_L) of the longest glacier length between this dataset (G_{Lmax}) and the RGI v6.0 (L_{max}).

In addition, the average value of positive D_L, the average value of negative D_L and the number of glaciers in different levels were calculated (Fig.12). The size of three pixels for DEM was used as the statistical tolerance, which means glaciers within the tolerance range were regarded as consistent extraction results. Statistically, there were 22017 glaciers within tolerance, 925 glaciers with negative D_L and 15111 glaciers with positive D_L that are greater than the tolerance. In terms of numerical comparison, G_{Lmax} obtained by our method was slightly larger than L_{max} in RGI v6.0.
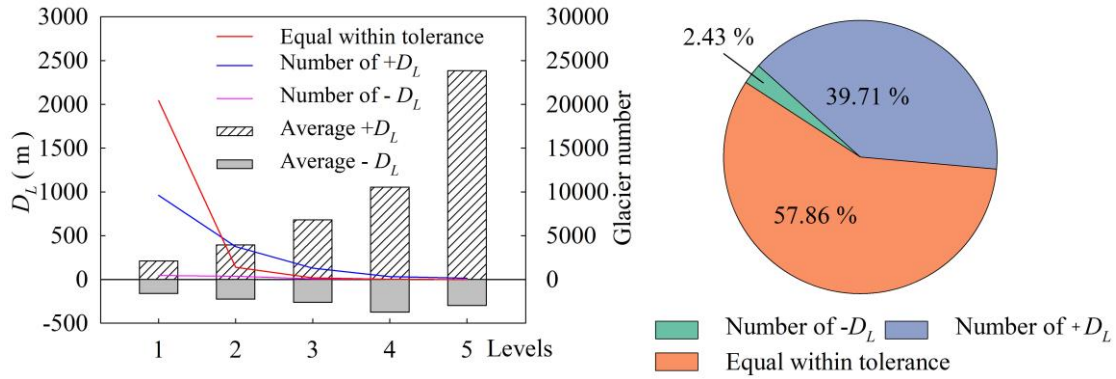
Figure 12: The statistical charts of the difference (D_L) of the longest length of glaciers by two methods in different glacier sizes.

4.4.2 Analysis of abnormal D_L

Combining the designed algorithm with visual inspection, the preliminary analysis showed that the local abnormal DEM, inaccurate glacier outlines and some glacier types (such as ice cap, slope glacier, etc.) were the main causes of abnormal D_L (Fig.13). Slope glacier is typical multi-origin and multi-exit glacier with almost the same number of local highest points and local lowest points, which often exist in pairs (Fig.13-a). If the local highest point did not match the local lowest point, a value of positive D_L would occur (Fig.13-a, blue polyline). Local abnormalities in DEM generally resulted in a shorter G_{Lmax} (negative D_L), as showed in Fig.13-b. Some key local highest points could not be identified because of the inaccurate outlines, resulting in a large negative D_L (Fig.13-c). For non-single glacier, this algorithm could only identify a lowest point, and all branches of glacier centerlines converge to this point, which would increase the length of most branches and make G_{Lmax} to be too large or even wrong (Fig.13-d).
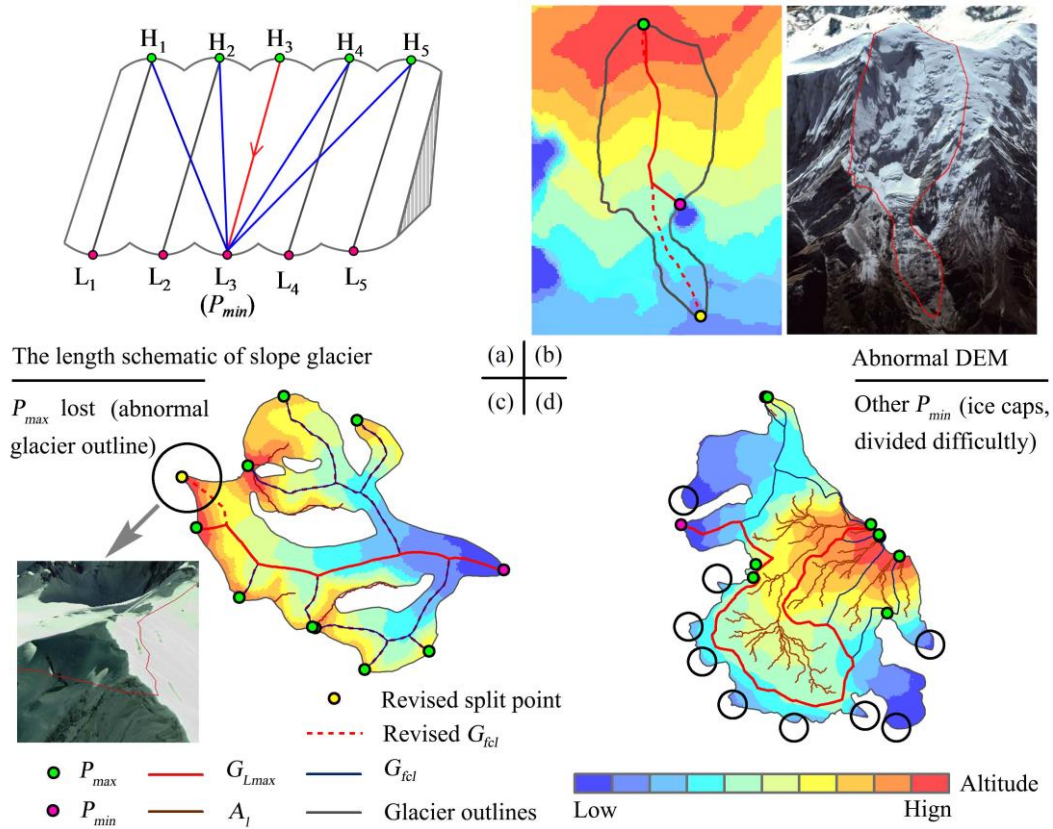
Figure 13: The schematic of probable causes for the abnormal of the longest glacier length. In Figure b, the red dashed line indicates the revised glacier centerline, and the yellow point is the correct lowest point (P_{min}). In Figure c, the red dashed line represents the missing branch, and the yellow point is a local highest point (P_{max}) missed by the algorithm. In Figure d, the black circle indicates some probable exits of the glacier, which needs to be divided into individual glaciers before extracting the centerlines.

The small or abnormal L_{max} of some glaciers was also the main reason of abnormal D_L. An abnormal example is shown in Fig.14. The Tugebieliqi Glacier (GLIMS_ID: G080334E42156N) with the maximum $|D_L|$ is the third largest glacier in China, behind the Sugatyanatjilga Glacier and the Tuomuer Glacier. Its G_{Lmax} was 40.179 km, but its L_{max} in the RGI v6.0 was only 11.703 km. The further measurement by Google Earth showed that the west-east length (D_{W-E}) of the glacier was about 27.72 km, which meant that our result was more conformable to reality.
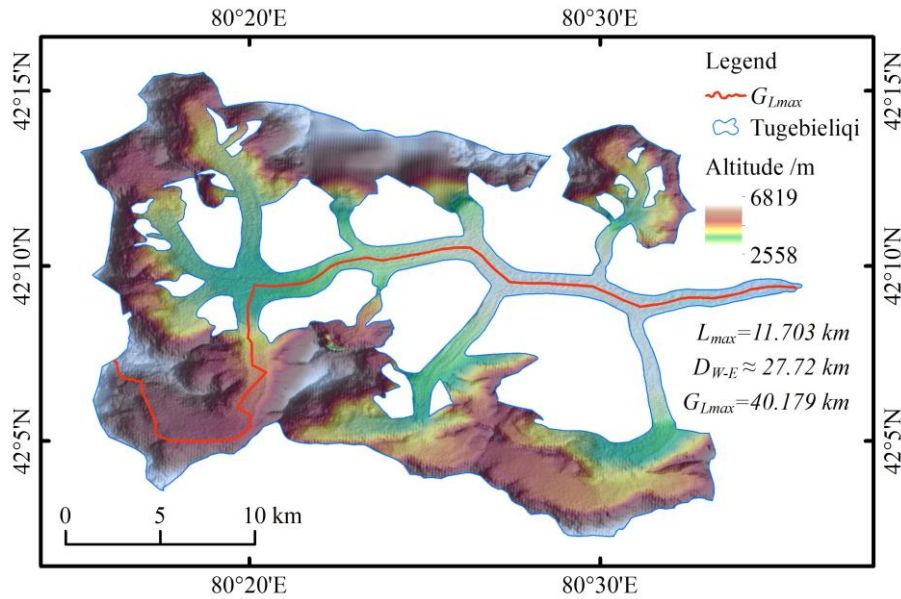
Figure 14: The schematic of the longest centerline of Tugebieliqi Glacier (L_{max}: the corresponding length of this glacier in the RGI v6.0; D_{W-E}: the distance from west to east of this glacier; G_{Lmax}: the length calculated by our method).

5 Discussion

5.1 Performance of the algorithm

In the process of extracting centerlines of glaciers in China, all glaciers were equally divided into eight tasks according to the number and considering the running efficiency of the algorithm. Based on the actual extraction results, five glaciers that failed to execute were added as the ninth task. Tasks coded T1~T9 were executed in the working environment of ArcGIS 10.4 software. Except for T7 and T9 using a Lenovo G410 (processors: Intel(R) Core(TM) i5-4210M CPU @ 2.60 GHz; memories: 4GB DDR3L 1600 MHz; video card: AMD Radeon R5 M230 2GB Discrete graphics) of home laptops, the other seven tasks used seven Dell OptiPlex 7040 (processors:Intel(R) Core(TM) i7-6700 CPU @ 3.40 GHz; memories: 8GB DDR4 2633 MHz; video card: AMD Radeon(TM) R5 340X 2GB Integrated graphics) of the tower server with the same configuration. The task distribution and execution results of the tests are given in Table 4.

Table 4 The statistics of assigning tasks and results of execution in tests.

Task ID	Assigned amount	Completed amount	Completion rate (%)	Total time (h)	Average time (s)
T1	6000	6000	100	31.00	18.60
T2	6000	6000	100	29.75	17.85
T3	6000	5999	99.98	30.53	18.32
T4	6000	6000	100	29.34	17.61
T5	6000	6000	100	33.54	20.12
T6	6000	5999	99.98	31.62	18.97
T7	6000	5999	99.98	58.63	35.18
T8	6571	6569	99.97	38.27	20.97
T9	5	5	100	0.12	86.26
Total	48571	48571	100	282.81	20.96

The results of the tests showed that the program took an average of 20.96 s to process an individual glacier, whereas it spent 86.26 s or even longer for some complex glaciers. Among the first eight processing tasks, T4 took the least time. The main reason was that the assigned glaciers in this task were mostly small and complex glaciers were less, except for the higher machine configuration. T7 took the longest time, and the cause was the lower machine configuration. The results of all tasks were merged to obtain the centerline dataset of the SCGI. It contained seven vector files (56 items) and nine logs, which took up about 912 MB in the storage.

5.2 Influence of glacier outline quality and DEM

The extraction method of glacier centerlines belongs to geometric graphic algorithm and depends on glacier outlines. Natively, comparing with the previous studies, our method has similar problems: (i) the delayed shunt and early convergence of the branches and (ii) the centerlines of same glacier in different periods, which is not geometrically comparable for some glaciers in drastic changes of outlines. The extraction results also showed that the branches of some glacier centerlines did have delayed diversion or early convergence, while the impact on the simulation of glacier's main flowline was limited. Considering that the results of extracting glacier centerlines change with the changes of glacier outlines, the measurement of the length change of glaciers in different periods will be the focus of our future work. We may further design a new algorithm to automatically supplement, extend, delete or modify the benchmarking glacier centerlines, so as to measure the changes of centerlines and length of glaciers in different periods.

360   Bare rock region refers to the non-glacial component that is within the outer boundary of the glacier outlines but is not covered by snow or ice. It can be divided into two types: one is the exposed rock protruding on the glacier surface; the other is the cliff generally existing between the upper part of the glacier and the firn basin. The snow or ice on the upper part of the glacier enters the firn basin through the cliffs. And the snow or ice on the cliffs are also important sources of replenishment for firn basin. So the cliffs are theoretically considered to be part of the glacier. However, the cliffs may be similar to the bare rock

365   area during the ablation season, and the cliffs are often accompanied by the presence of image shadows, which will easily cause misjudgments of glacier outlines in interpretation.

    Determining the ownership of bare rock regions in G_{fl} will improve the quality of glacier centerlines. In this study, all bare rock regions were considered to be the first category, and such cases were handled accordingly. The first category was divided

370   into two types: (i) the bare rock area on the upper part of the glacier being equivalent to the ice divide and (ii) the bare rock area near the end of the glacier. The attribution of most bare rock areas in the upper part of the glacier can be determined by the intersection point of A_l, G_{pl} with G_{br}. Only a few bare rock areas still exist alone, Eq. (12) was required to determine the segments of the G_{fl} to which they belong. Some bare rock areas located in the ablation area were allowed to exist alone in the G_{fl}, and the probability of their existence was extremely low.

375

    The determination of glacier's ELA is difficult. Some scholars believed that each glacier has its own ELA (Cui and Wang, 2013; Sagredo et al., 2016), but other scholars argued that the ELA of all glaciers in a certain region is the same (Sagredo et al., 2014; Jiang et al., 2018). The measurement of ELA requires continuous and long-term observation data, so it is very difficult to determine the ELA of the glaciers in large-scale. In this study, the ELA used to distinguish between the accumulation

380   area and the ablation area of the glacier was estimated by calculating the median of elevation (Z_{med}). For some glaciers (such as calving glaciers), the Z_{med} is above the actual ELA, which has been reasonably explained by scholars (Braithwaite and Raper, 2009). And it was considered that this overestimation is unlikely to affect the automatic calculation of glacier length (Machguth and Huss, 2014).

5.3 Some other factors influencing centerline of glaciers

385   Automatic extraction of glacier centerlines was basically carried out during the processing of polylines, so the processing algorithm of polylines in the program occupied a considerable part of codes. Among them, several common problems of disconnected polylines are shown in Fig.15. The following four types are important, which have a great influence on the accuracy and extraction automation of glacier centerlines.

390   (i) During the post-processing of the auxiliary lines, due to the inaccuracy of ice divide or the problems of DEM, the ridgelines in the edge of the ice divide of some glaciers start at the G_{pl} and end up with the G_{pl} or in parallel along the G_{pl}, which are unreasonable. In response to this problem, the algorithm set corresponding rules for screening in the processing of auxiliary lines, reducing the impact of such problems as much as possible.

    (ii) The visually closed vector polyline is not completely closed. Its start and end are at the same point, which is equal to a

395 natural division point. Unless the natural division point of G_{pl} completely coincides with a certain division point, the number of polyline records in the G_{pl} after division will be one more than we expected. Therefore, it is necessary to identify the natural division point during processing and merge the two disconnected polyline records.

    (iii) The algorithm of Euclidean allocation is accomplished based on raster operation, which is equivalent to the equidistant

400 scatter operation with the interval of P_8 on the glacier surface. For some glaciers with horizontal or vertical distribution of the G_{pl}, the extraction will continue after the centerlines overlaps with the G_{pl}. We only need to design the corresponding functions to detect and delete this redundancy of the disconnected polylines.

    (iv) In the process of calling the module of Euclidean allocation to generate the centerlines, there is a slight probability that

405 pixels with strictly equal distances will appear. The central axis will generate a regular rectangle based on the raster pixel corresponding to the central point, which will affect the calculation of the G_{Lmax}. In the algorithm, a function to identify and deal with such problems was added after the Euclidean allocation, then the polylines on one side of the diagonal of a rectangle were randomly retained.
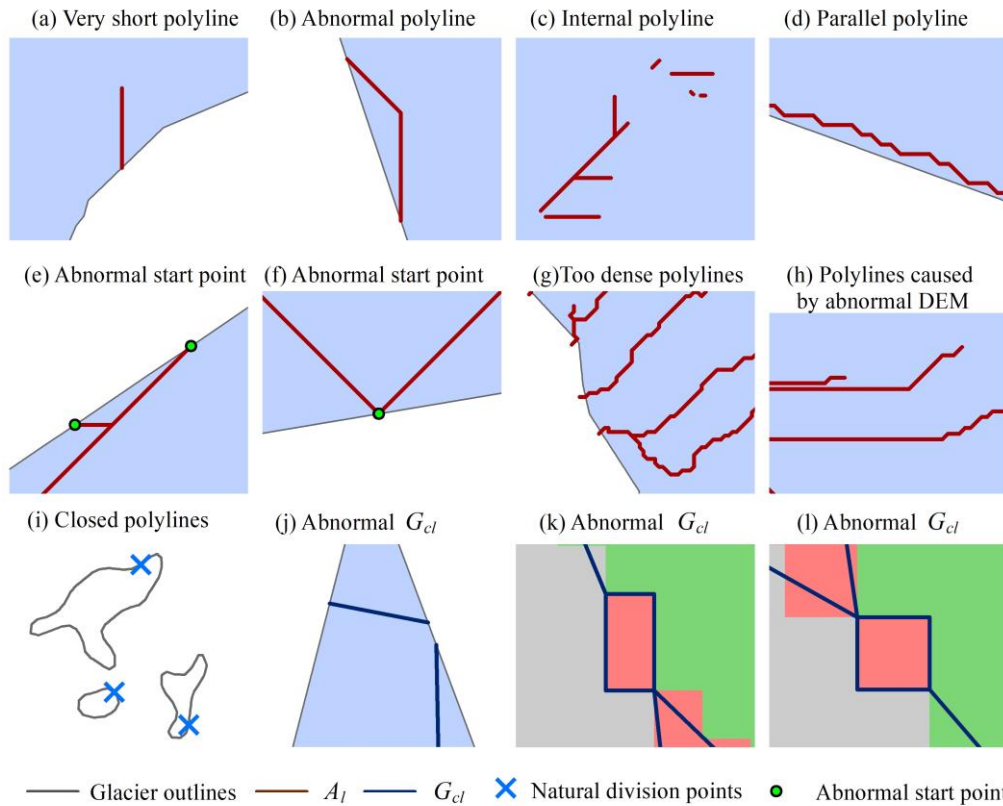
Figure 15: The schematic of discontinuous short polylines. Subgraphs a-h represent type (i), i represents type (ii), j represents type (iii) and k-l represent type (iv). The background in subgraphs a-h and j represent glacier-covered areas. Subgraph i shows several closed polylines, which does not fill background color. The different background colors in subgraphs k-l represent different areas of the glacier surface after the European allocation.

6 Conclusions

An automatic method for extracting glacier centerlines based on Euclidean allocation in two-dimensional space was designed and implemented in this study. It only needs the glacier outlines and the corresponding DEM to automatically generate the vector data of glacier centerlines, and provides different properties including the longest length, the average length, the length in the ablation region, the length in the accumulation region of the glacier. The standardized and automatic extraction of glacier centerlines requires no manual intervention. Meanwhile, we used the SCGI as the test data to run the program and verify its efficiency. The success rate of extracting glacier centerlines was very close to 100% and the comprehensive extraction accuracy

reached 94.34%, which reflected the robustness and simplicity of this method.

The automatic extraction algorithm proposed has three advantages: (i) introducing the auxiliary reference lines which ensure the validity of the upper glacier centerlines; (ii) success in automatically obtain the longest centerline of each glacier and the branches of glacier centerlines; (iii) providing more information of glacier lengths than other methods proposed by some scholars. Compared with the longest length of each glacier in the RGI v6.0, the length of the corresponding glacier calculated by our algorithm is in better agreement with the actual length of the glacier. We also identified the possible causes affecting the accuracy of glacier centerlines. In the future, we will focus on improving the time efficiency of the algorithm, providing the updated datasets of glacier centerlines with higher-quality, and identifying the abnormal glacier phenology such as glacier surging rapidly.

Appendix A

The paper uses numerous abbreviations. Explanations of main acronyms are listed in Table A1.

Table A1 The list of main acronyms in this study.

Acronyms	Description
A_t	The given area of an equilateral triangle
A_g	The polygon's area of the glacier's outer boundary
A_l	The final auxiliary line
A_r	The ridgelines of the glacier surface
G_{br}	The bare rock in glacier
G_{fcl}	The final glacier centerline
G_{fl}	The feature lines of glacier surface
G_{cl}	Glacier centerline
G_{Labl}	The length in the ablation region of the glacier
G_{Lacc}	The length in the accumulation region of the glacier
G_{Lmax}	The longest length of the glacier
G_{Lmean}	The average length of the glacier
G_{pl}	The polyline of the outer boundary of the glacier
G_{po}	The polygon of the outer boundary of the glacier
L_{max}	The longest glacier length of RGI v6.0
D_L	The difference between G_{Lmax} and L_{max}
P_t	The given perimeter of an equilateral triangle
P_g	The perimeter of the glacier's outer boundary
P_{max}	The local highest point of glacier outline
P_{min}	The lowest point of glacier outline
RGI	The Randolph Glacier Inventory
$SCGI$	The Second Chinese Glacier Inventory
Z_{med}	The median elevation of the glacier

Code availability

435   The code used to support the findings of this study are available from the corresponding author upon request.

Data availability

The datasets including the SCGI, RGI v6.0 and SRTM1 DEM v3.0 used in this study are freely available. The database of glacier centerlines in the SCGI produced in this study are available from the corresponding author upon request.

Author contribution

440   Xiaojun Yao designed this algorithm of extracting glacier centerlines and edited the manuscript. Dahong Zhang implemented the program and wrote the first draft of the manuscript. Hongyu Duan tested the program and checked the quality of glacier centerlines. Shiyin Liu, Wanqin Guo, Meiping Sun and Dazhi Li reviewed and edited the manuscript.

Competing interests

The authors declare that they have no conflict of interest.

445   **Acknowledgements**

We thank two reviewers for their valuable comments that improved the manuscript. Dahong Zhang thanks his current supervisor, Professor Shiqiang Zhang of Northwest University in Xi'an, China for valuable ideas and suggestions. This research was funded by the National Natural Science Foundation of China (No.41861013, No.42071089, No.41801052), the Open Research Fund of National Earth Observation Data Center (No. NODAOP2020007) and the Open Research Fund of National 450   Cryosphere Desert Data Center (No. 20D02).

References

Braithwaite, R. J., and Raper, S. C. B.: Estimating equilibrium-line altitude (ELA) from glacier inventory data, Annals of

Glaciology, 50, 127-132, doi: 10.3189/172756410790595930, 2009.

Cui, H., and Wang, J.: The methods for estimating the equilibrium line altitudes of a glacier, Journal of Glaciology and Geocryology, 35, 345-354, doi: 10.7522/j.issn.1000-0240.2013.0041, 2013.

Farr, T. G., Rosen, P. A., Caro, E., Crippen, R., Duren, R., Hensley, S., Kobrick, M., Paller, M., Rodriguez, E., Roth, L., Seal, D., Shaffer, S., Shimada, J., Umland, J., Werner, M., Oskin, M., Burbank, D., and Alsdorf, D.: The Shuttle Radar Topography Mission, Reviews of Geophysics, 45, 1-33, doi: 10.1029/2005rg000183, 2007.

Gao, Y. P., Yao, X. J., Liu, S. Y., Qi, M. M., Gong, P., An, L. N., Li, X. F., and Duan, H. Y.: Methods and future trend of ice volume calculation of glacier, Arid Land Geography, 41, 1204-1213, doi: 10. 12118 /j. issn.1000- 6060.2018.06. 08, 2018.

Gao, Y. P., Yao, X. J., Liu, S. Y., Qi, M. M., Duan, H. Y., Liu, J., and Zhang, D. H.: Remote sensing monitoring of advancing glaciers in the Bukatage Mountains from 1973 to 2018, Journal of Natural Resources, 34, 1666-1681, doi: 10.31497/zrzyxb.20190808, 2019.

Guo, W., Liu, S., Xu, J., Wu, L., Shangguan, D., Yao, X., Wei, J., Bao, W., Yu, P., Liu, Q., and Jiang, Z.: The second Chinese glacier inventory: data, methods and results, Journal of Glaciology, 61, 357-372, doi: 10.3189/2015JoG14J209, 2017.

Heid, T., and Kääb, A.: Repeat optical satellite images reveal widespread and long term decrease in land-terminating glacier speeds, The Cryosphere, 6, 467-478, doi: 10.5194/tc-6-467-2012, 2012.

Herla, F., Roe, G. H., and Marzeion, B.: Ensemble statistics of a geometric glacier length model, Annals of Glaciology, 58, 130-135, doi: 10.1017/aog.2017.15, 2017.

Ji, Q., Yang, T.-b., He, Y., Qin, Y., Dong, J., and Hu, F.-s.: A simple method to extract glacier length based on Digital Elevation Model and glacier boundaries for simple basin type glacier, Journal of Mountain Science, 14, 1776-1790, doi: 10.1007/s11629-016-4243-5, 2017.

Jiang, D. B., Liu, Y. Y., and Lang, X. M.: A multi-model analysis of glacier equilibrium line altitudes in western China during the Last Glacial Maximum, Science China Earth Sciences, 49, 1231-1245, doi: 10.1360/n072018-00058, 2018.

Kienholz, C., Rich, J. L., Arendt, A. A., and Hock, R.: A new method for deriving glacier centerlines applied to glaciers in Alaska and northwest Canada, The Cryosphere, 8, 503-519, doi: 10.5194/tc-8-503-2014, 2014.

Le Bris, R., and Paul, F.: An automatic method to create flow lines for determination of glacier length: A pilot study with Alaskan glaciers, Computers & Geosciences, 52, 234-245, doi: 10.1016/j.cageo.2012.10.014, 2013.

Leclercq, P. W., and Oerlemans, J.: Global and hemispheric temperature reconstruction from glacier length fluctuations, Climate Dynamics, 38, 1065-1079, doi: 10.1007/s00382-011-1145-7, 2012.

Leclercq, P. W., Pitte, P., Giesen, R. H., Masiokas, M. H., and Oerlemans, J.: Modelling and climatic interpretation of the length fluctuations of Glaciar Frías (north Patagonian Andes, Argentina) 1639–2009 AD, Climate of the Past, 8, 1385-1402, doi: 10.5194/cp-8-1385-2012, 2012a.

Leclercq, P. W., Weidick, A., Paul, F., Bolch, T., Citterio, M., and Oerlemans, J.: Brief communication "Historical glacier length changes in West Greenland", The Cryosphere, 6, 1339-1343, doi: 10.5194/tc-6-1339-2012, 2012b.

Leclercq, P. W., Oerlemans, J., Basagic, H. J., Bushueva, I., Cook, A. J., and Le Bris, R.: A data set of worldwide glacier length fluctuations, The Cryosphere, 8, 659-672, doi: 10.5194/tc-8-659-2014, 2014.

Li, H., Ng, F., Li, Z., Qin, D., and Cheng, G.: An extended "perfect-plasticity" method for estimating ice thickness along the flow line of mountain glaciers, Journal of Geophysical Research: Earth Surface, 117, 1020-1030, doi: 10.1029/2011jf002104,

2012.

Linsbauer, A., Paul, F., and Haeberli, W.: Modeling glacier thickness distribution and bed topography over entire mountain ranges with GlabTop: Application of a fast and robust approach, Journal of Geophysical Research: Earth Surface, 117, 3007-3024, doi: 10.1029/2011jf002313, 2012.

Liu, S. Y., Yao, X. J., Guo, W. Q., Xu, J. L., Shang Guan, D. H., Wei, J. F., Bao, W. J., and Wu, L. Z.: The contemporary glaciers in China based on the Second Chinese Glacier Inventory, Acta Geographica Sinica, 70, 3-16, doi: 10.11821/dlxb201501001, 2015.

Machguth, H., and Huss, M.: The length of the world's glaciers- a new approach for the global calculation of center lines, The Cryosphere, 8, 1741-1755, doi: 10.5194/tc-8-1741-2014, 2014.

McNabb, R. W., Hock, R., O'Neel, S., Rasmussen, L. A., Ahn, Y., Braun, M., Conway, H., Herreid, S., Joughin, I., Pfeffer, W. T., Smith, B. E., and Truffer, M.: Using surface velocities to calculate ice thickness and bed topography: a case study at Columbia Glacier, Alaska, USA, Journal of Glaciology, 58, 1151-1164, doi: 10.3189/2012JoG11J249, 2017.

Melkonian, A. K., Willis, M. J., and Pritchard, M. E.: Satellite-derived volume loss rates and glacier speeds for the Juneau Icefield, Alaska, Journal of Glaciology, 60, 743-760, doi: 10.3189/2014JoG13J181, 2017.

Muhuri, A., Natsuaki, R., Bhattacharya, A., and Hirose, A.: Glacier Surface Velocity Estimation Using Stokes Vector Correlation, Synthetic Aperture Radar, Singapore, 2015, 9781467372961, 606-609,2015.

Nuth, C., Kohler, J., König, M., von Deschwanden, A., Hagen, J. O., Kääb, A., Moholdt, G., and Pettersson, R.: Decadal changes from a multi-temporal glacier inventory of Svalbard, The Cryosphere, 7, 1603-1621, doi: 10.5194/tc-7-1603-2013, 2013.

Oerlemans, J.: A flowline model for Nigardsbreen, Norway: projection of future glacier length based on dynamic calibration with the historic record, Annals of Glaciology, 24, 382-389, doi: 10.1017/S0260305500012489 1997.

Paul, F., Barry, R. G., Cogley, J. G., Frey, H., Haeberli, W., Ohmura, A., Ommanney, C. S. L., Raup, B., Rivera, A., and Zemp, M.: Recommendations for the compilation of glacier inventory data from digital sources, Annals of Glaciology, 50, 119-126, doi: 10.3189/172756410790595778, 2009.

Sagredo, E. A., Rupper, S., and Lowell, T. V.: Sensitivities of the equilibrium line altitude to temperature and precipitation changes along the Andes, Quaternary Research, 81, 355-366, doi: 10.1016/j.yqres.2014.01.008, 2014.

Sagredo, E. A., Lowell, T. V., Kelly, M. A., Rupper, S., Aravena, J. C., Ward, D. J., and Malone, A. G. O.: Equilibrium line altitudes along the Andes during the Last millennium: Paleoclimatic implications, The Holocene, 27, 1019-1033, doi: 10.1177/0959683616678458, 2016.

Schiefer, E., Menounos, B., and Wheate, R.: An inventory and morphometric analysis of British Columbia glaciers, Canada, Journal of Glaciology, 54, 551-560, doi: 10.3189/002214308785836995 2008.

Sugiyama, S., Bauder, A., Zahno, C., and Funk, M.: Evolution of Rhonegletscher, Switzerland, over the past 125 years and in the future: application of an improved flowline model, Annals of Glaciology, 46, 268-274, doi: 10.3189/172756407782871143 2007.

Winsvold, S. H., Andreassen, L. M., and Kienholz, C.: Glacier area and length changes in Norway from repeat inventories, The Cryosphere, 8, 1885-1903, doi: 10.5194/tc-8-1885-2014, 2014.

Yang, B. Y., Zhang, L. X., Gao, Y., Xiang, Y., Mou, N. X., and Suo, L. D. B.: An integrated method of glacier length extraction

based on Gaofen satellite data, Journal of Glaciology and Geocryology, 38, 1615-1623, doi: 10.7522/j.issn.1000-0240.2016.0189, 2016.

Yao, X. J., Liu, S. Y., Zhu, Y., Gong, P., An, L. N., and Li, X. F.: Design and implementation of an automatic method for
530   deriving glacier centerlines based on GIS, Journal of Glaciology and Geocryology, 37, 1563-1570, doi: 10.7522/j. issn.1000-0240.2015. 0173, 2015.

Zhang, W., and Han, H. D.: A review of the ice volume estimation of mountain glaciers, Journal of Glaciology and Geocryology, 38, 1630-1643, doi: 10.7522 /j. issn.1000-0240.2016.0191, 2016.